Int. J. Heat Mass Transfer. Vol. 36, No. 3, pp. 577–591, 1993
Printed in Great Britain

0017-9310/93 $6.00 + 0.00

Computational study of laminar heat transfer downstream of a backward-facing step

T. KONDOH
Toyota Central Research and Development Labs, Inc., Nagakute-cho, Aichi-gun, Aichi Prefecture 480-11, Japan

and

Y. NAGANO and T. TSUJI
Department of Mechanical Engineering, Nagoya Institute of Technology, Gokiso-cho, Showa-ku, Nagoya 466, Japan

(*Received* 24 *January* 1992 *and in final form* 13 *April* 1992)

Abstract—Laminar heat transfer in a separating and reattaching flow was numerically studied by simulating the flow and heat transfer downstream of a backward-facing step. A series of computations was conducted in which three principal parameters governing the heat transfer in this geometry (i.e. channel expansion ratio *ER*, Reynolds number *Re* and Prandtl number *Pr*) were systematically changed. As a result, detailed relations between these parameters and the fundamental heat transfer characteristics have been elucidated. Some important findings are: (1) the distribution of the local Nusselt number depends strongly on all of these parameters; (2) the peak of the local Nusselt number does not necessarily locate at or very near the point of flow reattachment, in contrast to the common belief; and (3) if the Prandtl number is considerably low, the peak itself does not even appear and hence the heat transfer enhancement, usually assumed around the flow reattachment point, can never be expected in such cases.

1. INTRODUCTION

FLOW SEPARATION and subsequent reattachment exert an important influence on the mechanism of heat transfer. In some cases, they have a harmful effect such as uneven heat loading in thermal equipment, but in others, they produce a beneficial effect like heat transfer enhancement around the flow reattachment point. Thus, in engineering practice, it is quite essential to understand the basic mechanism of heat transfer in separating and reattaching flows.

A backward-facing step is one of the most fundamental geometries where the flow separation and reattachment occur, and accordingly, innumerable studies have been conducted in relation to this geometry. Nevertheless, most of them were concerned only with the flow, and our understanding of heat transfer seems still immature. Even at present, we have not fully settled the most fundamental problem, such as the question on the relation between the points of maximum heat transfer and flow reattachment.

Hitherto it has often been assumed that the peak of heat transfer occurs at or very near the point of flow reattachment. There are, however, several flaws in this assumption as recently presented by Sparrow and Chuck [1] and Sparrow *et al.* [2]. Their results, obtained both experimentally and numerically, indicate that this assumption is at best a special case. Sparrow and Chuck [1] also demonstrated firstly that the variation of the local Nusselt number with the Reynolds number took on different forms at various axial distances from the enlargement step. Although their results are very useful, the calculations covered rather limited ranges of the Reynolds number and the channel expansion ratio; besides, the influence of the Prandtl number was not considered at all.

In the present research, a more advanced study was undertaken on the heat transfer in laminar separating and reattaching flows. A series of computations was conducted in which three principal parameters governing the heat transfer in this geometry (i.e. channel expansion ratio *ER*, Reynolds number *Re* and Prandtl number *Pr*) were systematically changed. Special attention was paid to how the location of the maximum heat transfer relative to the flow-reattachment point varies with these parameters. In particular, the influence of the Prandtl number, never having been treated precisely although it is quite an important problem, was most extensively studied by dealing with its value ranging from quite low to extremely high.

2. GOVERNING EQUATIONS AND COMPUTATIONAL METHOD

The two-dimensional incompressible Newtonian flow with heat transfer was considered, which is

NOMENCLATURE

ER	channel expansion ratio, w_2/w_1
h	step height
Nu	local Nusselt number on heat transfer surface (lower wall downstream of step), $\alpha h/\lambda$
$\overline{Nu}$	mean of Nu in recirculating region, $\{\int_0^{X_R} Nu(x)\,dx\}/X_R$
Nu_0	Nu at step location ($x = 0$)
Nu_{max}	maximum of Nu
p	pressure
Pe	Peclet number, $Re\,Pr$
Pr	Prandtl number
Re	Reynolds number based on inlet flow velocity, $U_1 h/\nu$
T	temperature
t	time
T_1	temperature at inlet boundary
T_w	temperature of heat transfer surface (lower wall downstream of step)
U_1	external uniform velocity (in case of boundary layer type inflow) or mean velocity (in case of fully developed inflow) at inlet boundary
$\mathbf{u}$	velocity vector
w_1, w_2	channel widths upstream and downstream of step
X^*	x where local Nusselt number peaks (x for Nu_{max})
X_R	x where flow reattaches (x for flow reattachment point or flow reattachment length)
x	coordinate in mainstream direction with $x = 0$ at step location
y	coordinate perpendicular to mainstream direction with $y = 0$ at step bottom.

Greek symbols

α	local heat transfer coefficient on heat transfer surface (lower wall downstream of step), $-\lambda(\partial T/\partial y)_{y=0}/(T_w - T_1)$
δ_T	thickness of thermal boundary layer, $\int_0^{w_2} \theta\,dy$
θ	dimensionless temperature, $(T - T_1)/(T_w - T_1)$
λ	thermal conductivity
ν	kinematic viscosity
ρ	density.

Mathematical symbol

∇	vector differential operator, $\{\partial/\partial x, \partial/\partial y\}$.

described by the following equation of continuity (1), the Navier–Stokes equation (2) and the energy equation (3)

$$\nabla \cdot \mathbf{u} = 0 \tag{1}$$

$$\frac{\partial \mathbf{u}}{\partial t} + (\mathbf{u}\cdot\nabla)\mathbf{u} = -\nabla p + \frac{1}{Re}\nabla^2\mathbf{u} \tag{2}$$

$$\frac{\partial \theta}{\partial t} + (\mathbf{u}\cdot\nabla)\theta = \frac{1}{Re\,Pr}\nabla^2\theta. \tag{3}$$

In the above equations, t, ∇, $\mathbf{u}$, p and θ are the time, the vector differential operator, the velocity vector, the pressure and the temperature, respectively, all nondimensioned by the appropriate reference quantities. Re and Pr are the Reynolds and the Prandtl numbers.

Though only the steady-state solutions were desired, the time-dependent form of the equations was preferred so that they would be naturally realized as the asymptotic limit of the time-developing solutions. Thus, equations (2) and (3) were time-integrated to obtain the velocity and the temperature distributions, $\mathbf{u}$ and θ. As for the pressure distribution p, we used the Poisson form of the equation, which is derived from equations (1) and (2), and is expressed as

$$\nabla^2 p = -\nabla\mathbf{u} : (\nabla\mathbf{u})^* - \frac{\partial(\nabla\cdot\mathbf{u})}{\partial t} \tag{4}$$

where the superscript * denotes the transposition of a tensor and the colon represents the scalar product of two tensors, i.e.

$$\nabla\mathbf{u} : (\nabla\mathbf{u})^* = \left(\frac{\partial u}{\partial x}\right)^2 + 2\frac{\partial v}{\partial x}\frac{\partial u}{\partial y} + \left(\frac{\partial v}{\partial y}\right)^2. \tag{5}$$

The last term in the right-hand side of equation (4) including $\nabla\cdot\mathbf{u}$, called the dilatation term, was retained to compensate for the velocity field deviating from the continuity requirement (1).

The finite-difference method was employed to numerically solve the above equations. The spatial discretization was made on the nonstaggered (regular) grid, where the convection terms were discretized by the third-order-accurate upwind scheme [3], and the other spatial derivatives were evaluated by the central differences. The Crank–Nicolson scheme was used for the time integration. The matrix equations resulting from the discretization of the governing equations were solved with the successive over-relaxation method.

3. COMPARISON WITH PREVIOUS EXPERIMENTAL AND COMPUTATIONAL RESEARCH

Aung [4] conducted experiments on the laminar heat transfer in backward-facing step geometry for various step heights and the Reynolds numbers. For some of these measurements, Hall and Pletcher [5] performed comparative calculations using the viscous–inviscid interaction procedure, and Chiu and Pletcher [6] made a similar calculation based on the partially parabolized Navier–Stokes equation. Thus, in order to assure the reliability of the calculations, the predictions with the present method have been compared with these previous experiments and computations before carrying out a systematic numerical experiment.

Computations were made for two cases of step height, i.e. 6.4 and 12.7 mm, in Aung's experiment, where the channel width upstream of the step, w_1, was kept constant at 200 mm. The computational domain was set over 305 mm upstream of the step and 305 mm downstream thereof. The temperature throughout on the step-side (lower) wall was kept constant in accord with the experimental conditions. The momentum thickness of the boundary layer at the inlet boundary (305 mm upstream of the step) was specified, by referring to the conventional equation describing the development of the laminar boundary layer on a flat plate, so that the thickness of the boundary layer at the step location would match the measurement.

Figure 1 compares the temperature profiles in the recirculating region downstream of the step. In the case of a lower step height ($h = 6.4$ mm, $Re = 178$) shown in Fig. 1(a), the results of the present computation agree quite well with the experiment except for a slight difference near the wall at the section closest to the step ($x/X_R = 0.14$). In the case of a higher step height ($h = 12.7$ mm, $Re = 233$) shown in Fig. 1(b), some discrepancy exists between the calculations and the measurements in the middle of the recirculating region ($x/X_R = 0.482$ and 0.694). But the previous computations made by Hall and Pletcher [5] and Chiu and Pletcher [6] also suffer from a similar discrepancy, which might suggest that some experimental uncertainty is involved in the measurements. At the other two locations ($x/X_R = 0.946$ and 1.210), however, the present results agree well with the experimental data.

4. SYSTEMATIC NUMERICAL EXPERIMENT

There are three important parameters which exert a great influence on the fluid mechanics and heat transfer in a backward-facing step geometry, i.e. Reynolds number Re, channel expansion ratio ER and Prandtl number Pr. Thus, the influence of these parameters on the heat transfer has been studied by numerical simulation, in which the parameters were given the following values:

$$Re = \{10, 20, 50, 100, 200, 500\} \tag{6}$$

$$ER = \{1.25, 1.5, 1.67, 2\} \tag{7}$$

$$Pr = \{0, 0.0001, 0.001, 0.01, 0.04, 0.08, 0.1, 0.4, 0.7, 7, 10, 100, 1000\}. \tag{8}$$

As only the laminar flow was to be considered, the Reynolds number was examined up to 500. The channel expansion ratio was provided with four values. The Prandtl number was given a very wide range of values. The case of $Re = 100$, $ER = 1.5$ and $Pr = 0.7$ was taken as the reference condition, and each parameter was varied systematically.

The domain of computation was set over 10 step heights upstream of the step and 50 downstream thereof. The computational grid had nonuniform line spacings, having 60 grid lines in the mainstream direction and 30 across the channel. The grid lines were concentrated in the neighborhood of the wall, the minimum spacings of the grid being $\Delta x_{min} = 0.1$ in the mainstream direction and $\Delta y_{min} = 0.05$ in the transverse direction. To confirm the numerical accuracy, the line spacing was cut in half. Figure 2 shows the grid dependence of the calculated distributions of the local Nusselt number for the reference case ($Re = 100$, $ER = 1.5$, $Pr = 0.7$) and one of the most computationally difficult cases ($Re = 500$, $ER = 1.5$, $Pr = 7$). The broken lines correspond to the results obtained with a grid having twice as many (120 by 60) grid lines in each coordinate direction as the standard (60 by 30) grid. Evidently, the difference due to the grid fineness is very small, and hence the 60 by 30 grid was employed for computational efficiency in the following numerical experiment, except in the large Prandtl number cases ($Pr \geqslant 10$) for which the 85 by 60 grid was adopted. In this finer grid, the minimum spacings of the grid were $\Delta x_{min} = 0.02$ and $\Delta y_{min} = 0.01$. The adequacy of the spatial resolution in very high Prandtl number cases, especially in the transverse direction above the heat transfer surface, was confirmed in the following way: in the case of $Pr = 1000$ with $Re = 100$, where the temperature field was supposed to show the steepest spatial gradient of all the present numerical experiments, the computation was conducted with a coarser 60 by 40 grid. The results were compared with those of the 85 by 60 grid, but no essential differences were found between the two.

The boundary conditions were as follows: at the inlet boundary, the velocity field was assumed to be fully developed with the uniform temperature T_1, and the pressure boundary condition was specified as $\partial^2 p/\partial x^2 = 0$. At all of the wall boundaries, the no-slip condition was specified for the velocity. The pressure on the wall boundary was described by the momentum equation (2) with substitution of the no-slip boundary condition, i.e. $\partial p/\partial n = (1/Re)\partial^2 u_n/\partial n^2$, where n denotes the inward normal of the wall boundary. The

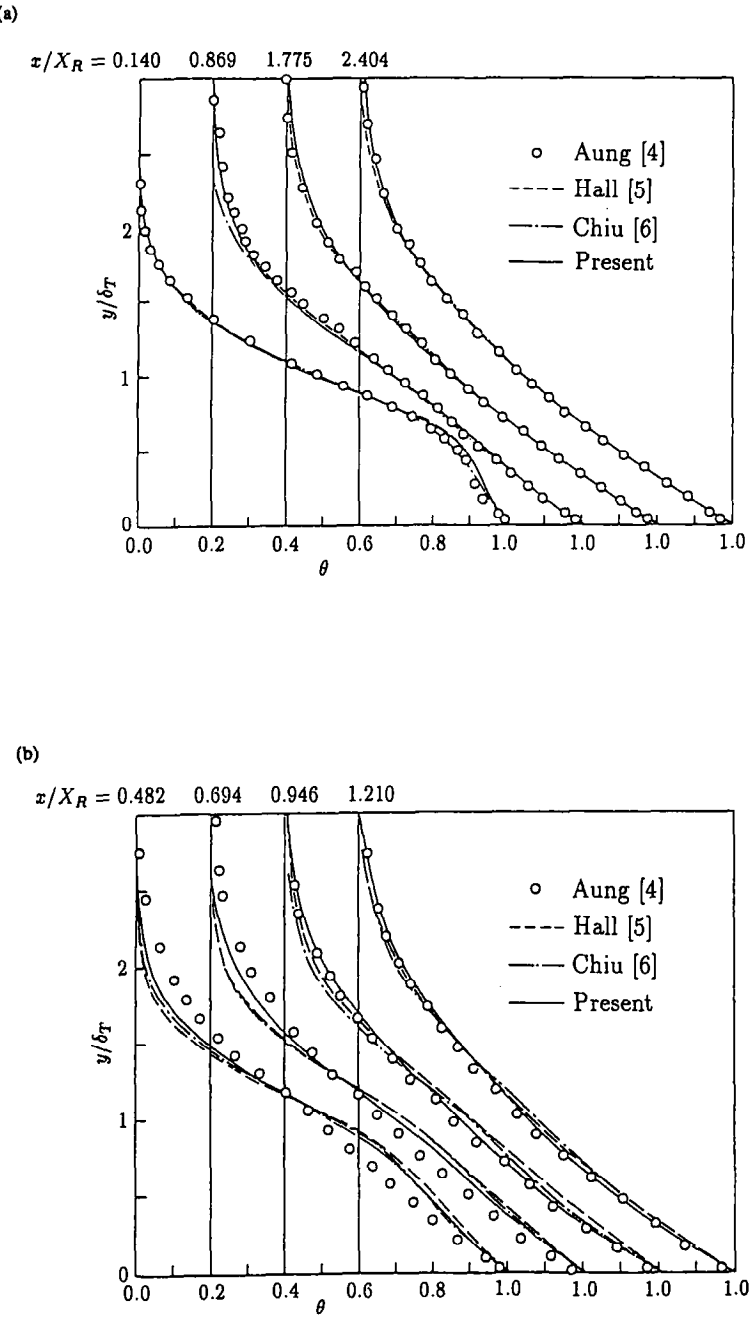

FIG. 1. Comparison of temperature profiles downstream of step with Aung's experiments: (a) $h = 6.4$ mm ($Re = 178$); (b) $h = 12.7$ mm ($Re = 233$).

temperature at the step-side (lower) wall downstream of the step was kept constant at T_w, which was assumed to be higher than T_1. The other part of the wall was treated as adiabatic. At the outlet boundary, the first derivative of the velocity and the second derivative of the temperature were assumed to vanish. The pressure was specified to be constant.

4.1. *Overview of velocity field*

The velocity field around the enlargement step calculated for the reference case (the channel expansion ratio of $ER = 1.5$ and the Reynolds number of $Re = 100$) is presented in Fig. 3. The flow-reattachment point is located at $x/h \approx 6.3$, as visualized by the dividing streamline superposed in the velocity

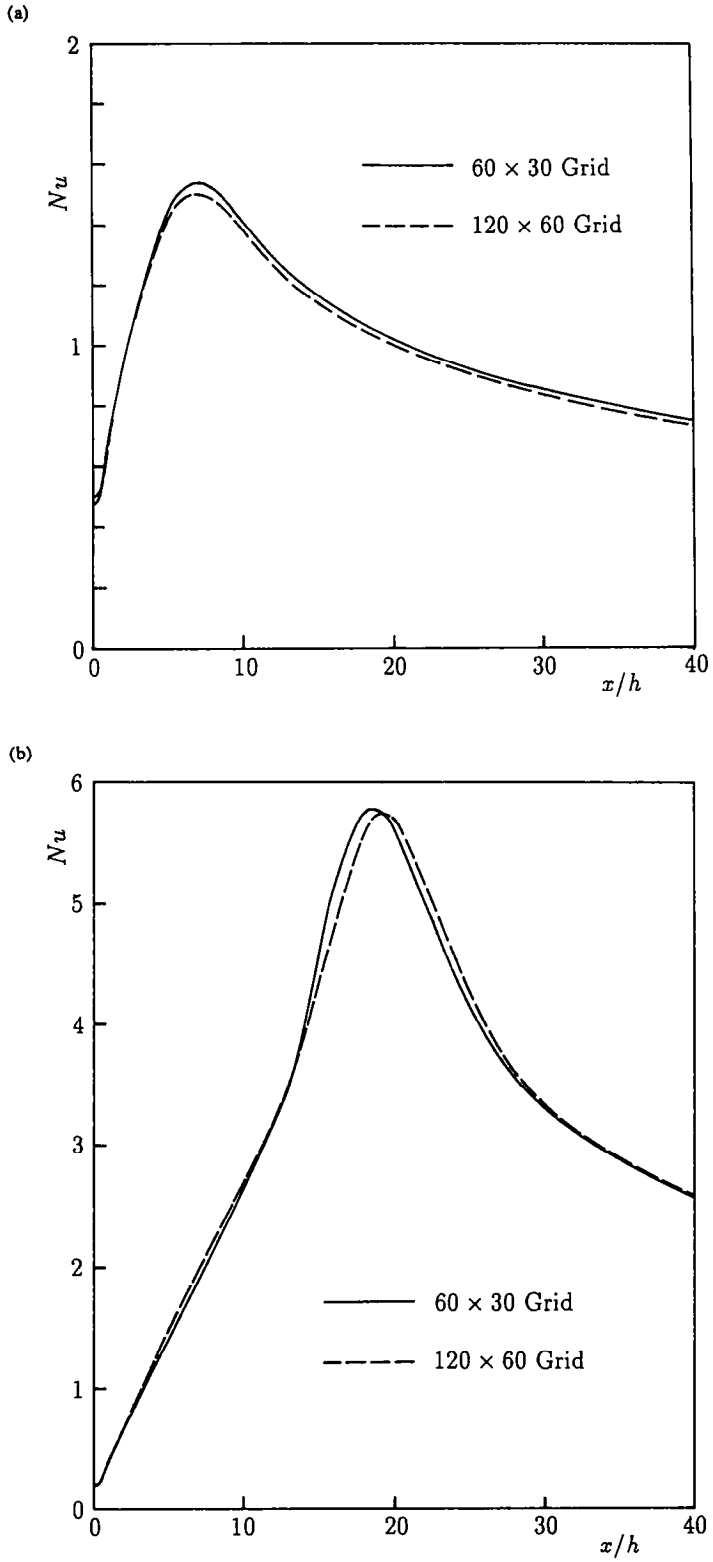

FIG. 2. Grid dependence of calculated distribution of local Nusselt number: (a) $Re = 100$, $ER = 1.5$, $Pr = 0.7$; (b) $Re = 500$, $ER = 1.5$, $Pr = 7$.

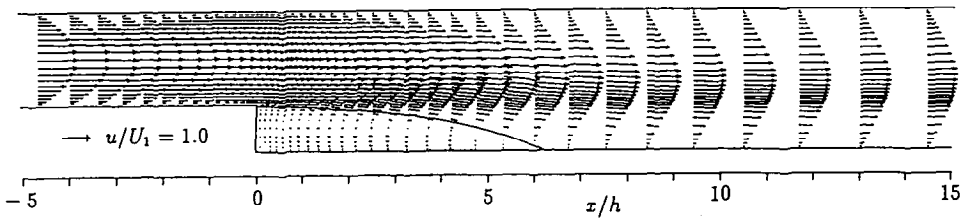

FIG. 3. Overview of velocity field ($ER = 1.5$, $Re = 100$).

vector distribution. The predicted reattachment length (6.3) is slightly longer than the experimental value of 6.0 [7]. But, because many of the earlier computations also gave a longer reattachment length than the experiment [7], some experimental uncertainty might be involved in the measurements. The flow in the recirculating region is very quiet, where the maximum reversed velocity is less than 10% of the mean velocity of the upcoming flow. This is quite in contrast to the turbulent flow case, where there is a strong and irregularly fluctuating flow [8]. After reattachment, the flow on the lower wall redevelops gradually to recover the fully developed state at $x/h \approx 15$.

4.2. *Influence of Reynolds number and channel expansion ratio*

Figure 4 shows the influence of the Reynolds number, Re, on the local heat transfer distribution. The channel expansion ratio, ER, and the Prandtl

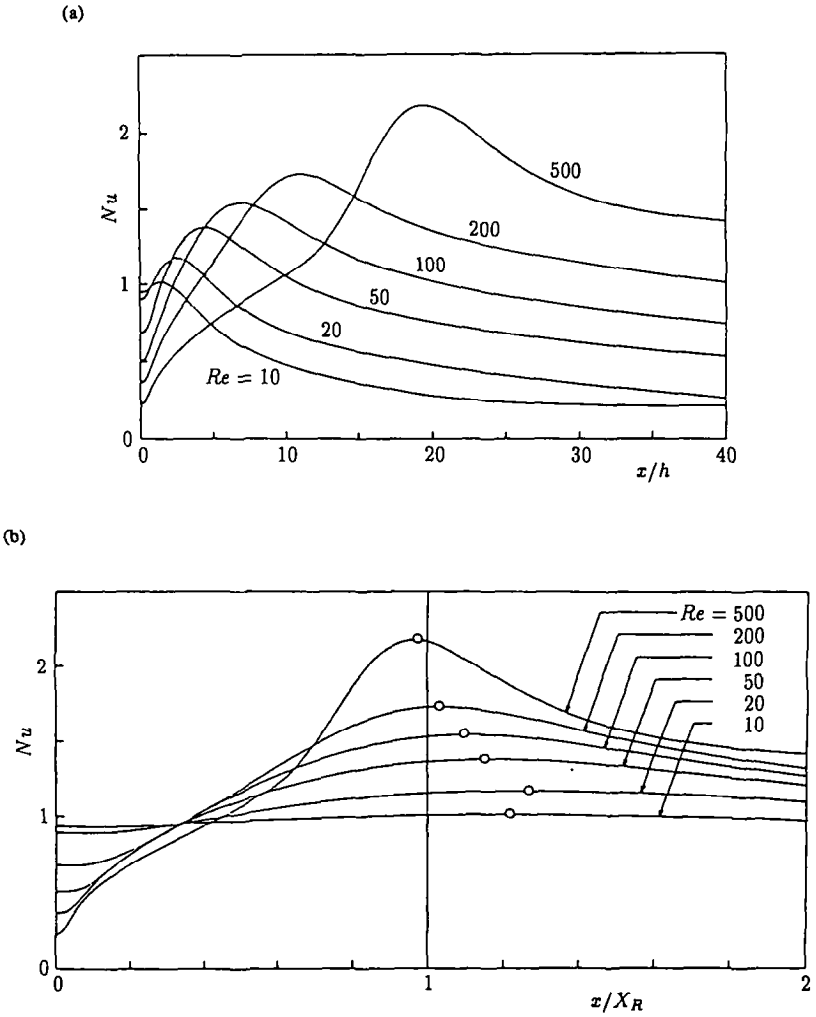

FIG. 4. Influence of Reynolds number on local heat transfer distribution ($ER = 1.5$, $Pr = 0.7$): (a) Nu vs x/h; (b) Nu vs x/X_R; (○) point of maximum heat transfer.

number, Pr, are fixed at 1.5 and 0.7, respectively, corresponding to the reference condition. The distribution of the local Nusselt number, Nu, on the heat transfer surface (lower wall downstream of the step) is shown in Fig. 4(a), in which the abscissa is the distance from the step normalized by the step height. For all of the Reynolds numbers, Nu first increases and then decreases. As the Reynolds number increases, the peak in the Nu distribution moves downstream accompanied by the consistently growing peak value. This movement of the peak values of Nu seems to be related to the movement of the flow-reattachment point. Thus, Nu is replotted in Fig. 4(b) with the abscissa (distance from the step) normalized by the flow reattachment length X_R. In contrast to the common belief, the peak value of Nu, indicated by the symbol 'O' in the figure, is not always located very near the flow-reattachment point. At $Re = 20$, for example, the distance between the peak location of Nu and the flow-reattachment point amounts to about 30% of the flow reattachment length. Figure 4 indicates that the relationship between these two locations depends considerably on the Reynolds number.

Figure 5 shows how the overall characteristics of the heat transfer vary with the Reynolds number. As the Reynolds number increases, the peak location of Nu relative to the flow-reattachment point, X^*/X_R, first moves downstream, and then moves back upstream beyond the flow-reattachment point. This movement of the peak location of Nu at higher Reynolds numbers is reasonable, since at much higher Reynolds numbers, i.e. in the turbulent flow case, the peak value of Nu is known to occur somewhat upstream of the flow-reattachment point [9]. The peak value of the Nusselt number, Nu_{max}, increases to the power of the Reynolds number, on the whole, and the mean Nusselt number in the recirculating region, $\overline{Nu}$, increases accordingly. The local Nusselt number in the upstream part of the recirculating region, on the other hand, as represented by the Nusselt number at the step location, Nu_0, decreases with the Reynolds number.

The variation of the overall heat transfer characteristics with the Reynolds number, described above, can be interpreted by the temperature distributions presented in Fig. 6. As shown in the figure, under the influence of the reattaching flow, the temperature contours undergo local distortion around the flow-reattachment point. In other words, the thermal boundary layer is compressed by the reattaching wallward flow. As a result, a layer with steep temperature gradient is formed above the wall around the flow-reattachment point, which leads to the heat transfer enhancement there. On the other hand, just behind the enlargement step, the temperature variation is concentrated in the separating shear layer, because the recirculating flow continues to convey there the high-temperature fluid generated on the heat transfer surface. Hence the temperature gradient just above the heat transfer surface becomes rather small, which results in the poor heat transfer there. These features of the temperature field become more distinct as the Reynolds number increases. This is why the overall characteristics of the heat transfer vary with the Reynolds number as in Fig. 5.

Figure 7 shows the influence of the channel expansion ratio, ER, on the local heat transfer distribution. The Reynolds number, Re, and the Prandtl number, Pr, are fixed at 100 and 0.7, respectively, corresponding to the reference condition. As ER increases, or equivalently, the upstream channel width decreases, the peak location of Nu moves upstream

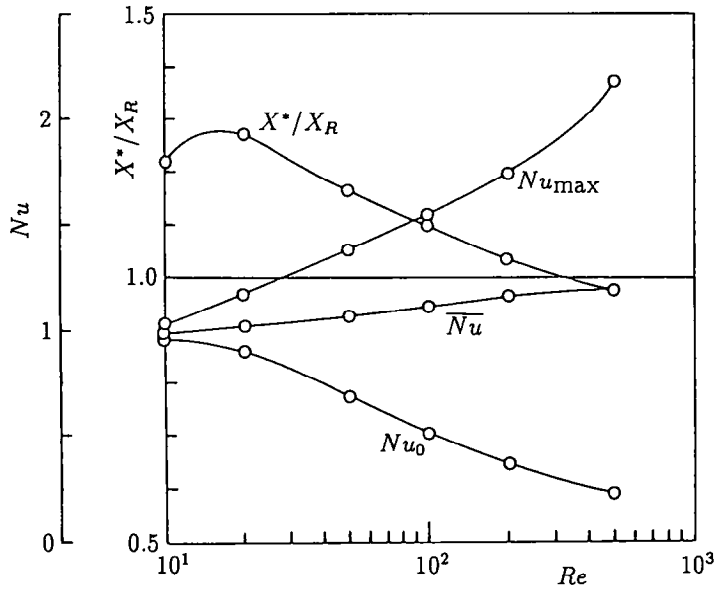

FIG. 5. Variation of heat transfer characteristics with Reynolds number ($ER = 1.5$, $Pr = 0.7$).

and the peak value grows consistently (Fig. 7(a)). This movement of the peak location of Nu is regarded again to be due to the movement of the flow-reattachment point, since the latter moves upstream with the increase of ER (not shown here). Then, Nu is replotted in Fig. 7(b) with the abscissa normalized by the flow reattachment length. It can be recognized that the peak value of Nu occurs slightly downstream of the flow-reattachment point and moves relatively closer to the flow-reattachment point as ER increases.

Figure 8 shows how the overall characteristics of the heat transfer vary with the channel expansion ratio. The peak value of the local heat transfer, Nu_{max}, increases consistently with ER. This is naturally understood by the fact that the compression of the thermal boundary layer by the reattaching flow becomes stronger with increasing ER as shown in Fig. 9. The mean Nusselt number in the recirculating region, $\overline{Nu}$, also increases with ER, but the Nusselt number in the upstream part of the recirculating region, Nu_0, decreases.

4.3. *Influence of Prandtl number*

The influence of the Prandtl number on the heat transfer in a separating and reattaching flow has not been studied extensively so far, although it seems quite

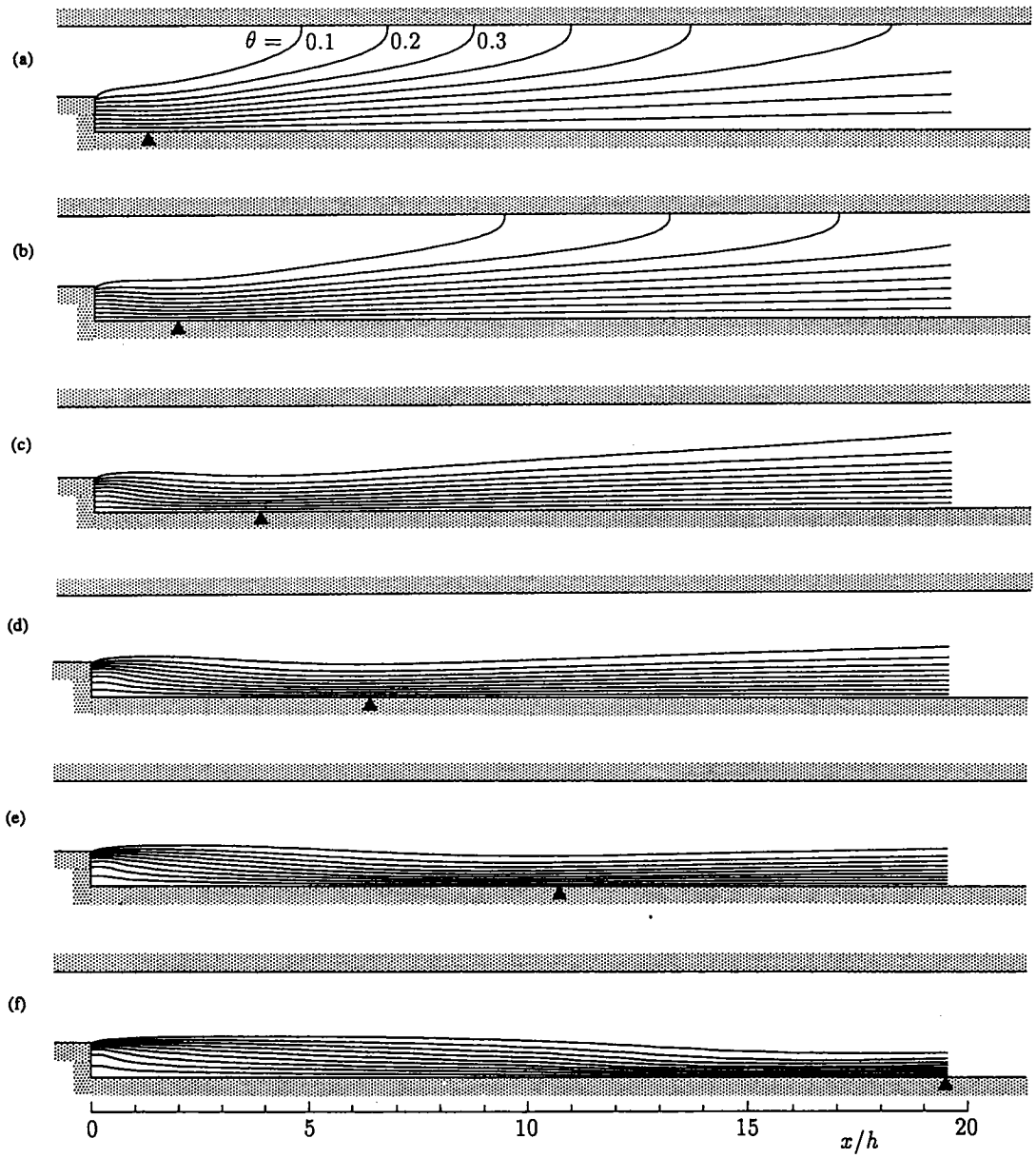

FIG. 6. Variation of temperature distribution with Reynolds number ($ER = 1.5$, $Pr = 0.7$): (a) $Re = 10$; (b) $Re = 20$; (c) $Re = 50$; (d) $Re = 100$; (e) $Re = 200$; (f) $Re = 500$; (▲) point of flow reattachment.

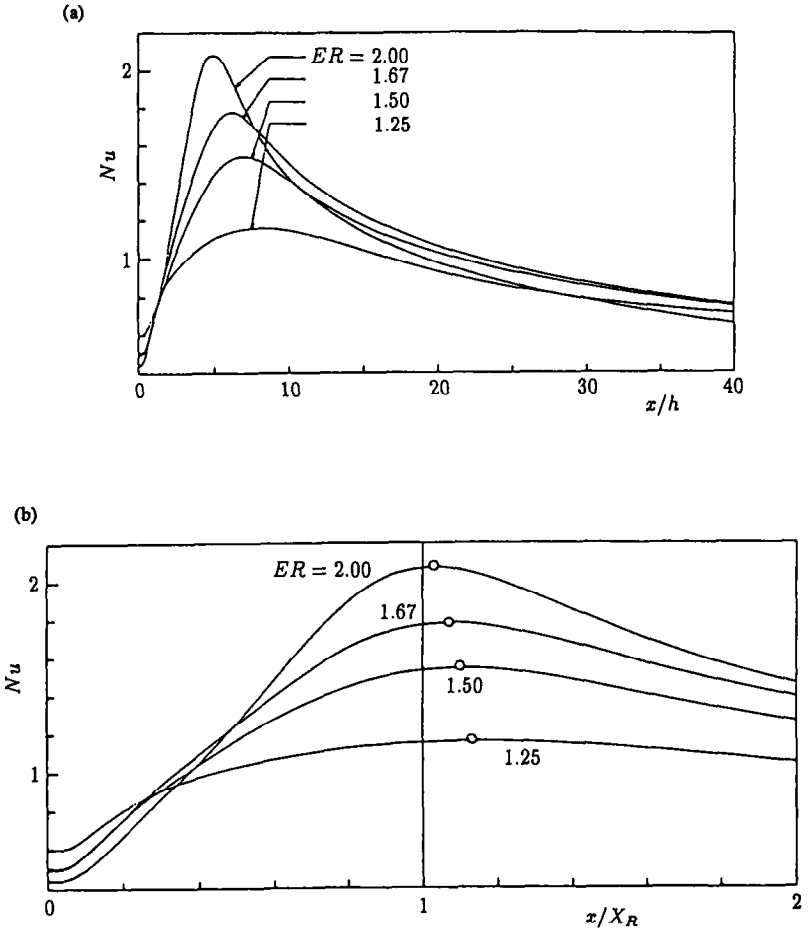

FIG. 7. Influence of channel expansion ratio on local heat transfer distribution ($Re = 100$, $Pr = 0.7$): (a) Nu vs x/h; (b) Nu vs x/X_R; (○) point of maximum heat transfer.

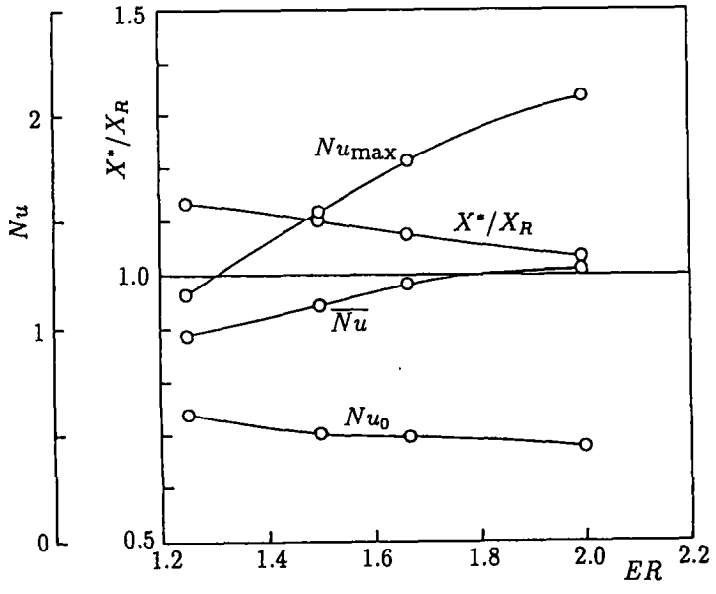

FIG. 8. Variation of heat transfer characteristics with channel expansion ratio ($Re = 100$, $Pr = 0.7$).

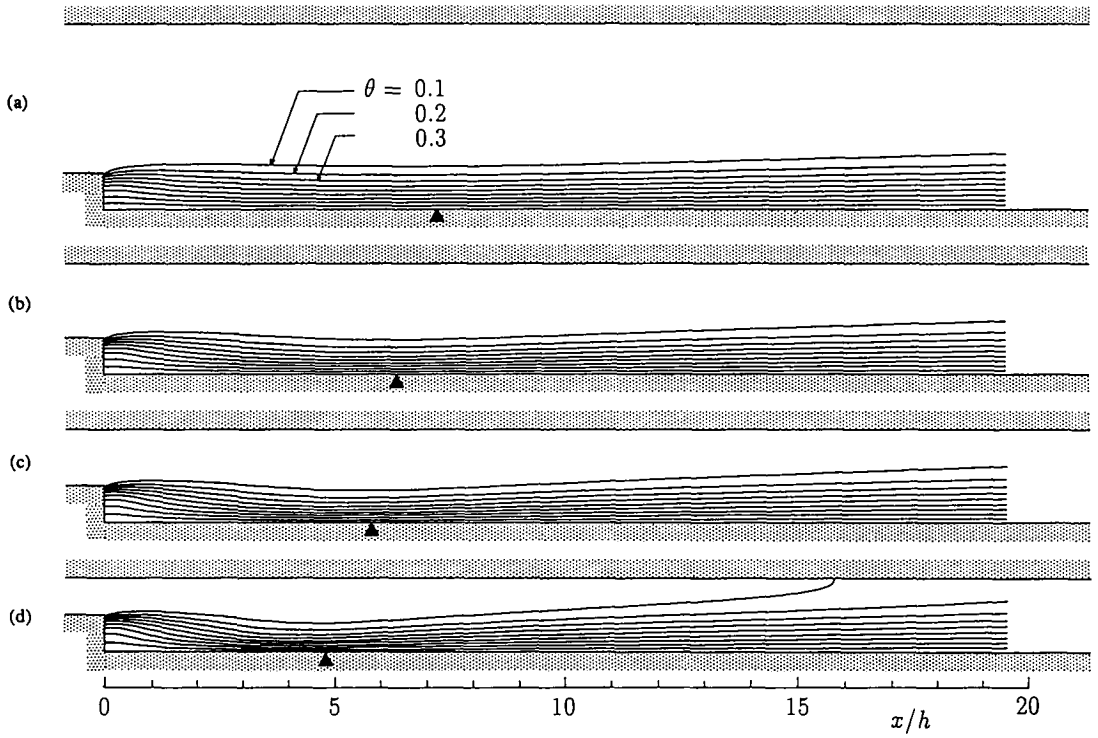

FIG. 9. Variation of temperature distribution with channel expansion ratio ($Re = 100$, $Pr = 0.7$): (a) $ER = 1.25$; (b) $ER = 1.50$; (c) $ER = 1.67$; (d) $ER = 2.00$; (▲) point of flow reattachment.

an important problem. One of the reasons for this may be the experimental difficulty in dealing with fluids having various Prandtl numbers. But today, as far as the laminar flow is concerned, it is not difficult to investigate the temperature field by numerical simulation. Thus, a series of computations has been conducted using Prandtl numbers ranging from quite low to extremely high, as indicated at the beginning of this section (see equation (8)). The Reynolds number, Re, and the channel expansion ratio, ER, were fixed at 100 and 1.5, respectively, corresponding to the reference condition. On the basis of the numerical results, the influence of the Prandtl number on the temperature distribution and the fundamental heat transfer characteristics was investigated in detail.

Figure 10 shows the temperature distribution for various Prandtl numbers. The curves in the figure correspond to the temperature contours with a non-dimensional temperature increment of $\Delta\theta = 0.1$. The following points describe how the temperature field changes with the Prandtl number.

(1) If the Prandtl number is considerably low, i.e. for $Pr \leqslant 0.001$ (or $Pe \leqslant 0.1$), the whole temperature field is governed by heat conduction. In this Prandtl number range, the influence of the heating surface (lower wall downstream of the step) reaches as far as the upcoming boundary, as shown in Figs. 10(b) and (c). Then the temperature distribution is substantially equal to the pure conduction field ($Pr = 0$) shown in Fig. 10(a), which was calculated from Laplace's equation ($\nabla^2\theta = 0$).

(2) In the Prandtl number range $0.001 \leqslant Pr \leqslant 0.1$ (or $0.1 \leqslant Pe \leqslant 10$), the temperature field receives the influence of both heat conduction and convection simultaneously. As shown in Figs. 10(d)–(f), the convection becomes more effective with an increase of the Prandtl number, which emerges as the behavior of the temperature contours in the main stream region moving downstream quite rapidly with the Prandtl number.

(3) For the Prandtl number range $0.1 \leqslant Pr \leqslant 1$ (or $10 \leqslant Pe \leqslant 100$), the convection effect becomes dominant in most of the region except in the recirculating region where the temperature is still largely controlled by heat conduction. In this Prandtl number range, the influence of the low-wall heating no longer reaches the upper wall (at least to the extent displayed in the figure), which leads to the formation of the temperature boundary layer above the heat transfer surface. This temperature boundary layer does not grow monotonically in the downstream direction, as visualized in Figs. 10(g) and (h); in fact, it is thinnest around the flow-reattachment point ($x/h = 6.3$).

(4) If the Prandtl number further increases, i.e. for $Pr \gtrsim 1$ (or $Pe \gtrsim 100$), the temperature field is governed much more by convection; the thermal layers are formed here and there, i.e. on the heat transfer surface, on the side surface of the step, and also in the separating shear layer just behind the step, as shown

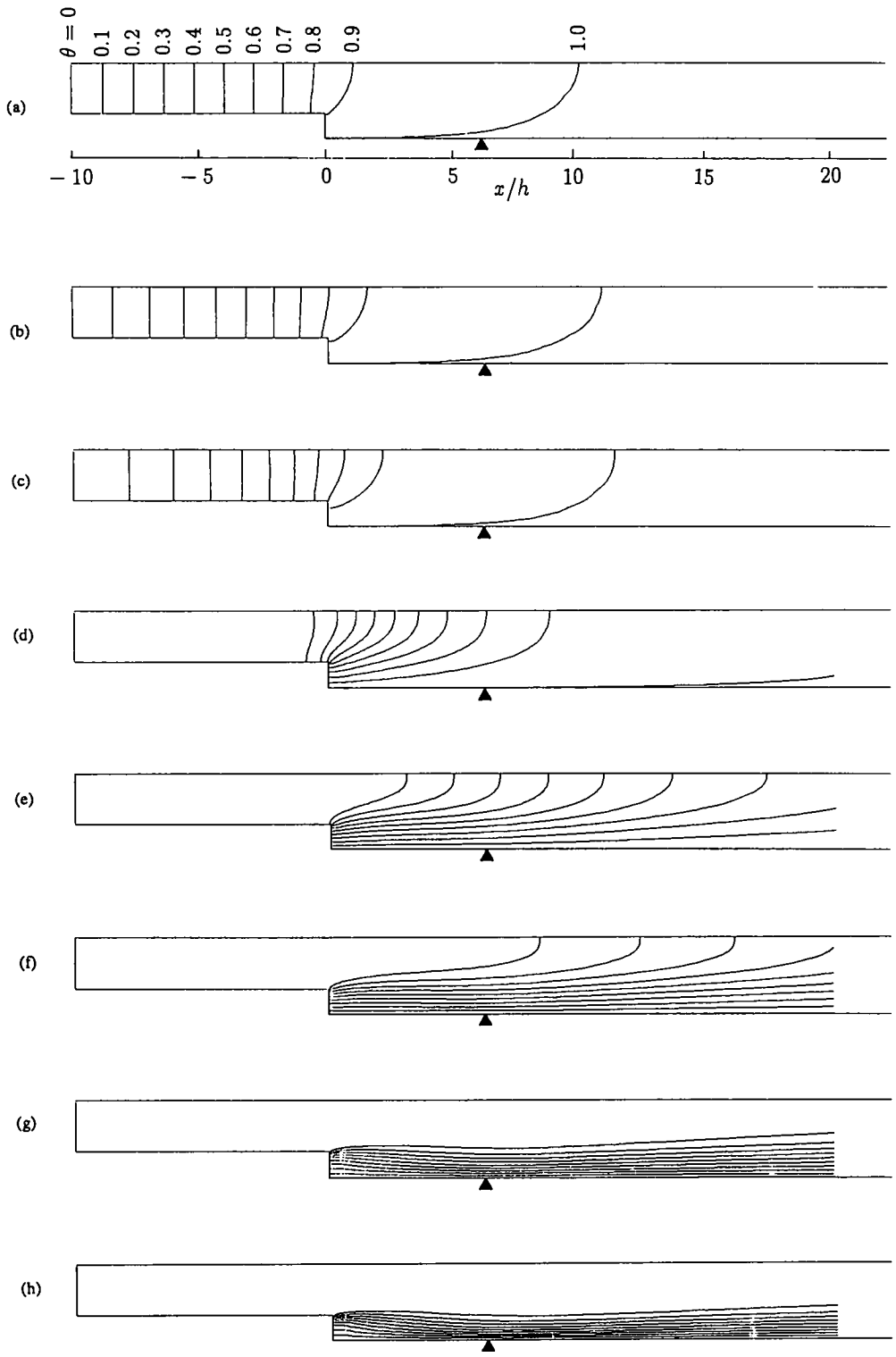

FIG. 10. Temperature distribution for various Prandtl numbers: (a) $Pr = 0$; (b) $Pr = 0.0001$; (c) $Pr = 0.001$; (d) $Pr = 0.01$; (e) $Pr = 0.04$; (f) $Pr = 0.1$; (g) $Pr = 0.4$; (h) $Pr = 0.7$; (i) $Pr = 10$; (j) $Pr = 100$; (k) $Pr = 1000$; lines correspond to temperature contours with nondimensional temperature increment of $\Delta\theta = 0.1$; (▲) point of flow reattachment.

(*Continued over*)

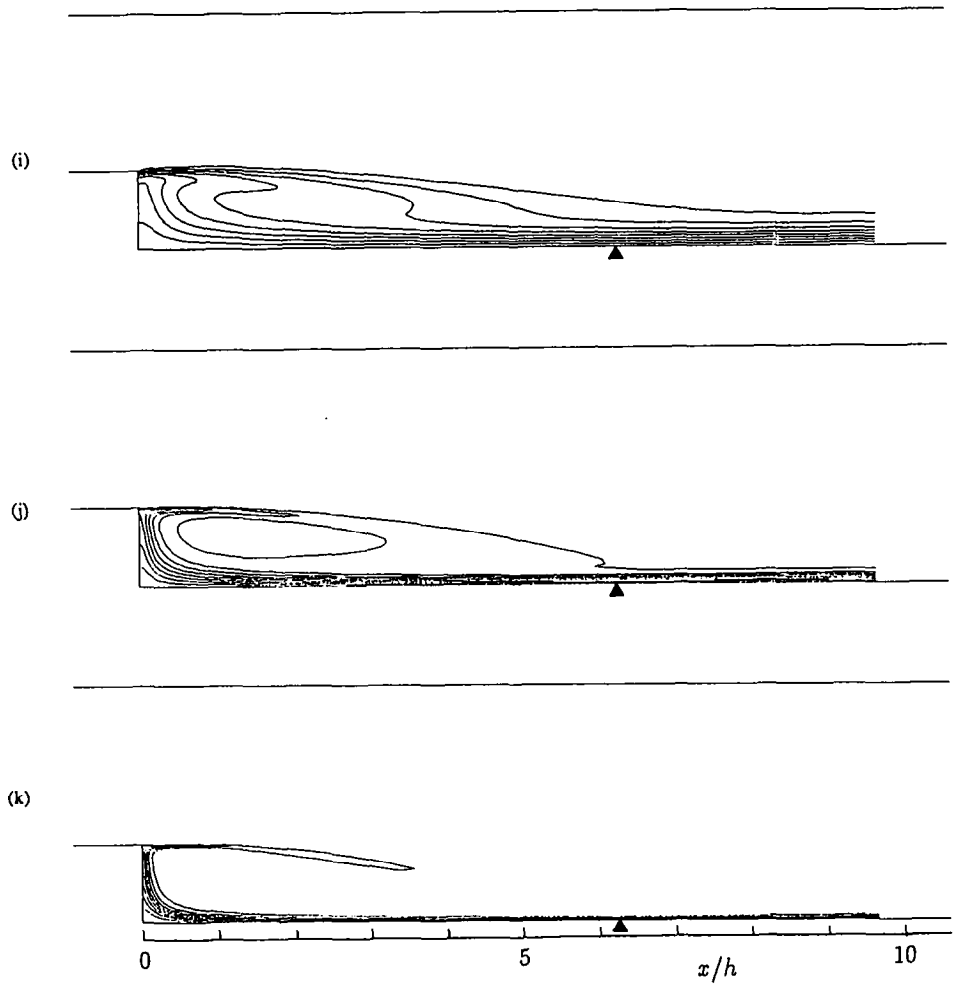

FIG. 10.—*Continued.*

in Figs. 10(i) and (j). The more the Prandtl number increases, the thinner these thermal layers become, as shown in Fig. 10(k).

Figure 11 shows how the 'thermal front', defined here as the external or upstream boundary of the region where the influence of heating surface reaches, varies with the Prandtl number. The lines in the figure indicate the contours of nondimensional temperature $\theta = 0.01$ for various Prandtl numbers. For $Pr \leqslant 0.001$, as stated above, the influence of the heating surface reaches as far as the upstream incoming boundary. When the Prandtl number increases to 0.04, the thermal front descends to the step location. Then, in the Prandtl number range $0.1 \leqslant Pr \leqslant 0.7$, it moves further downstream quite rapidly with the Prandtl number. At a Prandtl number greater than 1, the thermal boundary layer appears above the heat

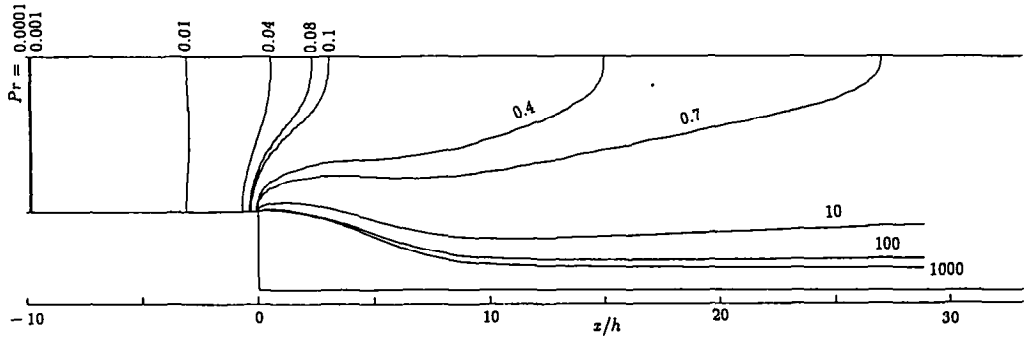

FIG. 11. External bound of region which receives influence of heating surface for various Prandtl numbers ($Re = 100$, $ER = 1.5$): lines correspond to contours of nondimensional temperature $\theta = 0.01$.

transfer surface. The thickness of the layer decreases consistently with the Prandtl number.

Figure 12 shows the local heat transfer distribution for various Prandtl numbers, in which the local Nusselt number on the heat transfer surface, Nu, is plotted against the distance from the step normalized by the step height. The following are remarkable features of the local heat transfer distribution.

(1) For $Pr \leqslant 0.001$ (or $Pe \leqslant 0.1$), the distribution of Nu does not differ essentially from the pure conduction case ($Pr = 0$), which again confirms that the temperature field is substantially governed by heat conduction.

(2) For $0.001 \leqslant Pr \leqslant 0.1$ (or $0.1 \leqslant Pe \leqslant 10$), the influence of convection begins to appear in the distribution of Nu, but the effect of the reattaching flow is still too weak to bring about substantial heat transfer enhancement around the flow-reattachment point. At $Pr = 0.01$, the distribution of Nu becomes slightly different in quantity from the $Pr = 0$ case, but it is not in quality; at $Pr = 0.04$, there appears firstly an inflection point in the distribution of Nu, which means that the effect of compression of the thermal boundary layer by the reattaching flow begins to work. As the Prandtl number increases, Nu increases in the whole region and the pattern of the Nu distribution changes from the monotonically decreasing one into the one having a local maximum around the flow-reattachment point.

(3) For $Pr \gtrsim 0.1$ (or $Pe \gtrsim 10$), the substantial heat transfer enhancement by the reattaching flow is recognized around the flow-reattachment point. At $Pr = 0.1$, the local maximum of Nu around the flow reattachment point is approximately comparable with Nu_0 (i.e. Nu at the step location) which has occupied the global maximum in the lower Prandtl number range; Nu continues to increase with the Prandtl number in the whole region and the heat transfer enhancement around the flow-reattachment point becomes more and more remarkable.

It is usually assumed, in the separating and reattaching flows, that heat transfer is generally enhanced around the flow-reattachment point. However, the present numerical experiment demonstrated that this is not always true; the relation between the points of flow reattachment and maximum heat transfer depends quite strongly on the Prandtl number. Under the conditions considered in the present investigation, substantial heat transfer enhancement never occurred for a Prandtl number less than 0.1.

Figure 13(a) shows how the maximum Nusselt number, Nu_{max}, changes with the Prandtl number in its range where substantial heat transfer enhancement is recognized, i.e. for $Pr \gtrsim 0.1$. As shown in the figure, Nu_{max} increases roughly to the power of the Prandtl number as $Nu_{max} \propto Pr^{0.35}$. Figure 13(b) shows how the mean Nusselt number in the recirculating region, $\overline{Nu}$, changes with the Prandtl number. The variation of $\overline{Nu}$ with the Prandtl number is divided into three

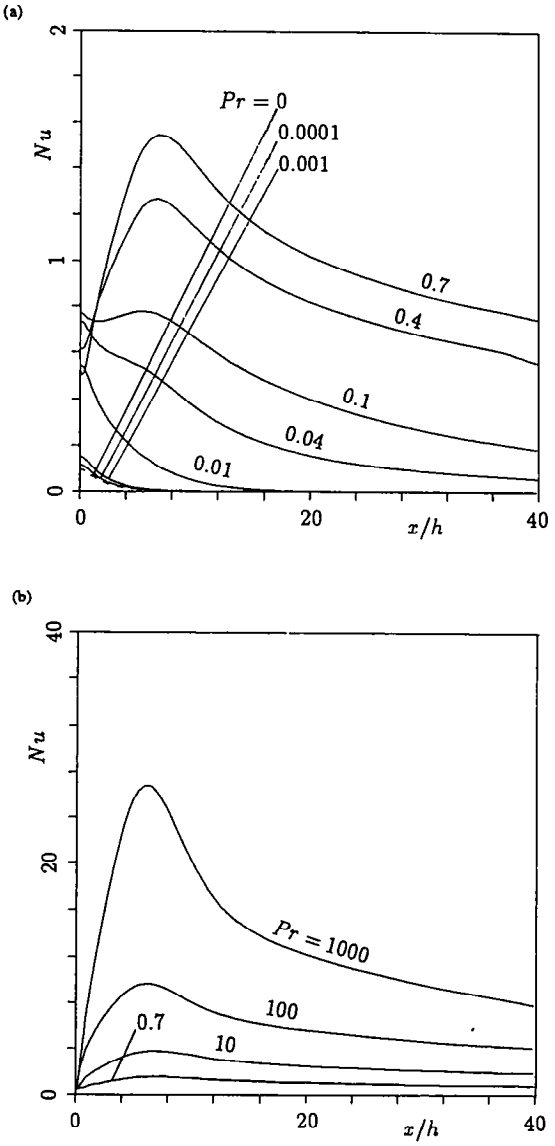

FIG. 12. Local heat transfer distribution for various Prandtl numbers ($Re = 100$, $ER = 1.5$): (a) $Pr = 0$–0.7; (b) $Pr = 0.7$–1000.

parts. Referring to the temperature distribution shown in Fig. 10, the heat transfer mechanism in each part is considered.

(1) The first is the part $Pr \leqslant 0.001$ (or $Pe \leqslant 0.1$), where the heat transfer rate stays at quite a low level, being substantially equal to that of pure conduction, and hardly changes with the Prandtl number. As already stated repeatedly, this is because the temperature field is substantially governed by heat conduction.

(2) The second is the part $0.001 \leqslant Pr \leqslant 0.1$ (or $0.1 \leqslant Pe \leqslant 10$), where $\overline{Nu}$ increases quite rapidly with the Prandtl number. In this Prandtl number range, under the influence of convection which becomes more and more effective with the Prandtl number, the

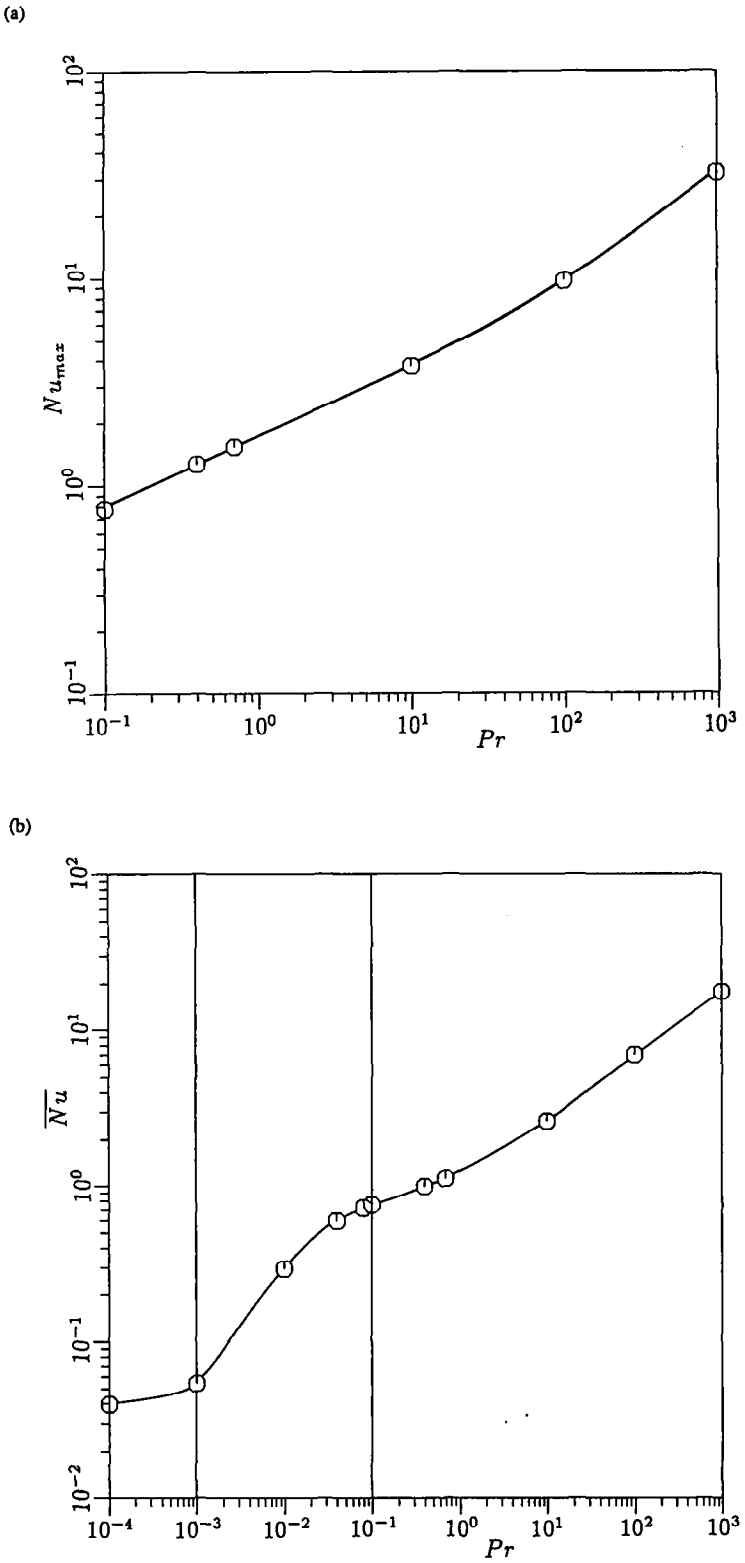

FIG. 13. Variation of heat transfer characteristics with Prandtl number ($Re = 100$, $ER = 1.5$) : (a) maximum Nusselt number; (b) mean Nusselt number in recirculating region.

temperature contours are forced to contract above the heat transfer surface. And in addition, the surface area, which contributes to substantial heat transfer in the recirculating region, is urged to spread. As a result, $\overline{Nu}$ increases quite rapidly with the Prandtl number. The increase of the heat transfer in this mechanism continues until $Pr \approx 0.1$, when $\overline{Nu}$ reaches the level of 1.0. This value of $\overline{Nu}$ is reasonable because it can occur if the temperature contours line up horizontally with the vertically constant interval behind the step as realized in Fig. 10(f).

(3) The third is the part $Pr \gtrsim 0.1$ (or $Pe \gtrsim 10$), where the usually assumed heat transfer enhancement by the reattaching flow really occurs. Although the increase of $\overline{Nu}$ by the previously mentioned mechanism halts around $Pr = 0.1$, $\overline{Nu}$ begins to increase again by a different mechanism, i.e. compression of the thermal boundary layer by the reattaching flow. When the Prandtl number increases beyond unity, the effect of convection in the recirculating region further accelerates the increase of $\overline{Nu}$.

5. CONCLUSIONS

The laminar heat transfer in a separating and reattaching flow was numerically studied by simulating the flow and heat transfer downstream of the backward-facing step. A series of computations was conducted in which three principal parameters governing the heat transfer in this geometry (i.e. channel expansion ratio ER, Reynolds number Re and Prandtl number Pr) were systematically changed. As a result, detailed relations between these parameters and the fundamental heat transfer characteristics have been elucidated.

The influences of the Reynolds number and the channel expansion ratio were investigated at a moderate value of the Prandtl number, i.e. $Pr = 0.7$. The heat transfer enhancement by the reattaching flow was observed in all cases treated here. But, in contrast to the common belief, the peak of the local Nusselt number did not necessarily locate at or very near the point of the flow reattachment. Moreover, it was demonstrated that the relative location of this peak against the flow-reattachment point varies considerably depending upon both the Reynolds number and the channel expansion ratio.

The influence of the Prandtl number was most extensively studied in terms of its range from quite low to extremely high, where the Reynolds number and the channel expansion ratio were fixed at 100 and 1.5, respectively. The important features of the Prandtl number influence on the heat transfer are:

(1) if the Prandtl number is considerably low, i.e. for $Pr \lesssim 0.001$ (or $Pe \lesssim 0.1$), the whole temperature field is substantially governed by heat conduction;

(2) for a Prandtl number less than 0.1 (or $Pe \lesssim 10$), heat transfer enhancement, usually assumed around the flow reattachment point, either does not occur, or is not essential; and

(3) only for the Prandtl number greater than 0.1 (or $Pe \gtrsim 10$) can substantial heat transfer enhancement be realized, where the heat transfer rate increases roughly to the power of the Prandtl number; for example, the peak value of the local Nusselt number increases with the Prandtl number as $Nu_{max} \propto Pr^{0.35}$.

REFERENCES

1. E. M. Sparrow and W. Chuck, PC solutions for heat transfer and fluid flow downstream of an abrupt, asymmetric enlargement in a channel, *Numer. Heat Transfer* **12,** 19–40 (1987).
2. E. M. Sparrow, S. S. Kang and W. Chuck, Relation between the points of flow reattachment and maximum heat transfer for regions of flow separation, *Int. J. Heat Mass Transfer* **30,** 1237–1246 (1987).
3. T. Kawamura and K. Kuwahara, Computation of high Reynolds number flow around a circular cylinder with surface roughness, AIAA Paper 84-0340 (1984).
4. W. Aung, An experimental study of laminar heat transfer downstream of backsteps, *J. Heat Transfer* **105,** 823–829 (1983).
5. E. J. Hall and R. H. Pletcher, Application of a viscous–inviscid interaction procedure to predict separated flows with heat transfer, *J. Heat Transfer* **107,** 557–563 (1985).
6. I.-T. Chiu and R. H. Pletcher, Prediction of heat transfer in laminar flow over a rearward-facing step using the partially-parabolized Navier–Stokes equations, *Proc. 5th Int. Heat Transfer Conf.*, pp. 415–420. Hemisphere, Washington, D.C. (1986).
7. K. Morgan, J. Periaux and F. Thomasset (Eds), *Analysis of Laminar Flow over a Backward Facing Step: A GAMM Workshop*, Vol. 9 of *Notes on Numerical Fluid Mechanics*. Friedr. Vieweg, Braunschweig (1984).
8. T. Kondoh and Y. Nagano, Numerical investigation of three-dimensional separating and reattaching flow downstream of a backward-facing step. In *Numerical Methods in Fluid Dynamics* (Edited by M. Yasuhara, H. Daiguji and K. Oshima), pp. 263–270. Japan Society of Computational Fluid Dynamics, Yoshinodai (1989).
9. J. C. Vogel and J. K. Eaton, Combined heat transfer and fluid dynamic measurements downstream of a backward-facing step, *J. Heat Transfer* **107,** 922–929 (1985).